IL NUOVO CIMENTO **38 C** (2015) 65
DOI 10.1393/ncc/i2015-15065-6

COMMUNICATIONS: SIF Congress 2014

Search for Dark Matter direct production in the monophoton plus missing transverse momentum final state in *pp* collisions at $\sqrt{s} = 8\,\text{TeV}$ with the ATLAS detector

M. M. PEREGO

CEA/IRFU, Centre d'etude de Saclay - University Paris Sud, France

received 31 January 2015

Summary. — This paper presents a search for dark matter pair production in association with an energetic photon in $20.3\,\text{fb}^{-1}$ of pp collisions collected at $\sqrt{s} = 8\,\text{TeV}$ by the ATLAS detector at the LHC. The final state investigated in this analysis is defined by large missing transverse momentum ($E_T^{miss} > 150\,\text{GeV}$) and by the presence of an energetic photon ($p_T > 125\,\text{GeV}$). Observations in data are compared to the Standard Model expectations and no significant excess is found. A model-independent limit is set on the presence of new physics in data. Data are also interpreted in the framework of effective field theories which describe the interaction between dark matter and incoming partons as a contact interaction parameterized by a set of dimensional operators.

PACS 14.70.Bh – Photons.
PACS 95.35.+d – Dark matter (stellar, interstellar, galactic, and cosmological).

1. – Introduction

Several astrophysical and cosmological observations indicate the existence of a new non-barionic matter, the dark matter (DM), which predominantly constitutes galaxies and the other structures in the universe [1]. However, its identity is still unknown. One of the most promising DM candidates is a weakly interacting massive particle (WIMP), which is a thermal relic of the early universe. At the LHC it is possible to look for WIMPs (χ) direct production. Once produced in the collisions, if stable enough, the DM particles escape the detector without leaving any trace or any energy deposits, since they are neutral and feebly interacting. Their presence may be inferred from an imbalance in the visible transverse momentum, hence their main signature is large missing transverse momentum $E_{\text{T}}^{\text{miss}}$. A Standard Model (SM) particle from initial state radiation (ISR) is required to tag these events, otherwise invisible. If the mediator M of the interaction between SM and DM particles is much heavier than the momentum transfer of the interaction, it is possible to describe the interaction in the effective field theories (EFT)

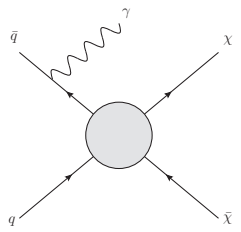

Fig. 1. – WIMP pair production via an effective interaction. A photon is radiated from initial state quarks.

framework by integrating out the mediator and considering a contact interaction (fig. 1). Limits can be set on the two theory parameters: M^* ($M^* = \frac{M}{\sqrt{g_{SM}\, g_\chi}}$, where g_{SM} and g_χ are the couplings of the mediator to SM particles and DM particles, respectively) and the dark matter mass m_χ.

2. – The LHC and the ATLAS detector

The Large Hadron Collider (LHC) is a proton and heavy ions accelerator built in a circular underground tunnel located at CERN. It consists of a 27-kilometer ring of superconducting magnets and accelerating cavities to boost the energy of the particles along the way. Inside the accelerator, two high-energy proton beams travel at relativistic speeds and they collide in four points. The four interaction points are surrounded by the LHC experiments: ATLAS [2] and CMS [3] are multipurpose experiments, designed to study high transverse momentum events for the search of the Higgs boson and phenomena beyond the Standard Model. LHCb [4] is an experiment devoted to the b-quark physics study and CP violation studies while ALICE [5] is designed to analyze lead ion collisions. The LHC is designed to provide proton-proton collisions at a nominal center-of-mass energy of 14 TeV and its design instantaneous luminosity is $1 \times 10^{34}\,\mathrm{cm}^{-2}\mathrm{s}^{-1}$. In 2012 the center of mass energy was 8 TeV, the beam bunches spacing time was 50 ns and the peak luminosity $\sim 8 \times 10^{33}\,\mathrm{cm}^{-2}\mathrm{s}^{-1}$.

2˙1. *The ATLAS detector system.* – ATLAS (A Toroidal LHC Apparatus) is a giant detector with a cylindrical symmetry around the beam line [2]. A right-handed coordinate system is used in ATLAS: the nominal interaction point is defined as the origin of the coordinate system, the z-axis is defined by the beam direction and the x-y plane is transverse to the beam direction. The positive x-axis is defined as pointing from the interaction point to the center of the LHC ring and the positive y-axis is defined as pointing upwards. The azimuthal angle ϕ is measured around the beam axis, and the polar angle θ is the angle from the beam axis. Polar angle quantities are expressed in terms of pseudorapidity, defined as $\eta = -\log(\tan(\frac{\theta}{2}))$. Transverse quantities, such as the transverse momentum p_T ($p_T = P\sin(\theta)$, where P is the absolute value of the momentum of the particle) and the missing transverse momentum E_T^{miss}, are defined in the x-y plane. The distance ΔR in the pseudorapidity-azimuthal angle space is defined as: $\Delta R = \sqrt{\Delta\eta^2 + \Delta\Phi^2}$.

ATLAS is built as a series of different sub-detectors devoted to detect particles exploiting their different interaction with matter. Starting from the interaction point there is the tracker, the electromagnetic calorimeter, the hadronic calorimeter and the muon spectrometer.

The inner part of the detector is the Inner Detector (ID) which is a tracking detector [6]. The ID is devoted to the measurement of charged particles tracks. The solenoidal magnetic system is essential for momentum measurement of charged particles and for the reconstruction of secondary vertices. The ID has an acceptance in pseudo-rapidity of $|\eta| < 2.5$ for particles coming from the interaction region while it has a full coverage in Φ. The detectors dedicated to measure the energy of the particles (apart from muons) and their position are the calorimeters. The calorimetric system is composed by an electromagnetic compartment, dedicated to the measurements of electrons and photons, and an hadronic compartment, suited for jet reconstruction. For precise missing transverse momentum measurements a full coverage in pseudorapidity (extending up to $|\eta| < 4.9$) is provided. The Electromagnetic Calorimeter (EM) is a sampling calorimeter built as a LAr (liquid argon) ionization chamber with lead absorbers. It is composed of two half-barrels, which cover the pseudorapidity range $|\eta| < 1.37$, and two endcap regions, covering the range $1.52 < |\eta| < 2.37$. The region where $1.37 < |\eta| < 1.52$ is called "crack region" and it suffers from a poor performance because of the ID services passing through. The EM calorimeter is longitudinally segmented in three sections, called *strips*, *middle* and *back* sections with a different segmentation in the $\eta \times \Phi$ plane. An additional very thin ($\sim 1\,\mathrm{mm}$) layer is set in front of the EM calorimeter to recover the energy lost by electrons and photons in the material before the calorimter. The calorimeter relative energy resolution, after noise subtraction, is parametrised with the expression: $\frac{\sigma(E)}{E} = \frac{a}{\sqrt{E}} \oplus c$, where E is in GeV, $a \sim 10\%$–$17\%[\sqrt{\mathrm{GeV}}]$ and $c \sim 0.7\%$ [7]. The ATLAS hadronic calorimeter detector consists of the Tile calorimeter (made of layers of scintillator material and iron) in the central region, liquid argon hadronic endcap calorimeter (HEC) and liquid argon forward calorimeter (FCal). The energy resolution of the barrel and endcap detectors is $\frac{\Delta E}{E} = \frac{50\%}{\sqrt{E[\mathrm{GeV}]}} \oplus 3\%$, while the energy resolution for the forward calorimeter is $\frac{\Delta E}{E} = \frac{100\%}{\sqrt{E[\mathrm{GeV}]}} \oplus 10\%$. The muon detector surrounds the calorimeters. It is a muon spectrometer (MS) consisting of three air-core superconducting magnet systems. The MS has a separate trigger covering the region $|\eta| < 2.4$ and high-precision tracking chambers covering the pseudorapidity region $|\eta| < 2.7$.

3. – Object reconstruction

3˙1. *Electrons and photons.* – Electrons and photons reconstruction is seeded by the presence of a cluster in the EM calorimeter. Electrons, being charged particles, leave also a track in the inner detector pointing to the cluster. On the contrary, a cluster with no tracks pointing to it can be classified as an unconverted photon candidate (*i.e.* a photon not converted into an electron-positron pair). The experimental signature of a converted photon is the presence of two tracks coming from a secondary vertex pointing to the cluster [8]. Once reconstructed, photons are subject to photon identification which aims to discriminate real photons from fake photons originating, for example, from narrow and electromagnetic-like jets. The photon identification process is based on variables which describe the electron/photon shower profile (both longitudinal and transverse) in the EM calorimeter. Photons are required to have isolation energy (energy in calorimeters in a cone of radius $\Delta R = 0.4$ around the cluster after candidate energy subtraction) less than 5 GeV (isolated photons).

3˙2. *Jets.* – Jets are reconstructed from noise suppressed cluster of energy in the calorimeters using the anti-k_t algorithm [9] with a radius parameter $R = 0.4$.

3˙3. *Muons.* – Muons are reconstructed by combining tracks and energy deposits in the MS and ID systems, or are required to have an ID track which is extrapolated to the MS and it is associated with at least one track segment in the MS [10].

3˙4. *Missing transverse momentum* E_T^{miss}. – The vector momentum imbalance in the transverse plane is called missing transverse momentum and is defined as the negative vector sum of the reconstructed and calibrated physics objects in the event [11]. For the $E_{\mathrm{T}}^{\mathrm{miss}}$ computation, calorimeter cells are associated to reconstructed and identified high p_T objects in a specific order: electrons, photons, taus, jets, muons. Energy deposits not associated to high p_T objects are added using an energy flow algorithm [11].

4. – Analysis strategy

The monophoton analysis is a counting experiment: it aims to count the number of observed events in a Signal Region (SR) in data and to compare it to the Standard Model prediction.

The Standard Model processes which contribute to the monophoton SR mainly come from electroweak processes. The dominant source of background ($\sim 70\%$) is given by $Z(\nu\nu)+\gamma$ processes: neutrinos coming from the Z decay produce large missing transverse momentum and the photon is produced in association with the boson. $W(l\nu)+\gamma$ processes enter the SR ($\sim 15\%$) either if the lepton is missed or reconstructed as a photon, or if the τ lepton is hadronically decaying. In addition Z/W + jets processes where the jet is reconstructed as a photon (*jet faking photon*) or where the electron fakes a photon (*electron faking photon*) contribute as $\sim 10\%$. Smaller contributions come from $Z(ll)+\gamma$, where both leptons are missed ($\sim 0.3\%$), $\gamma+jet$ events, where a jet is partially lost faking high E_T^{miss} ($\lesssim 0.1\%$), dibosons, $t\bar{t}$ and single-t processes. The estimation of $Z/W+\gamma$ contributions is based on the definition of Control Regions (CR) (*i.e.* background-like regions enriched in a certain source of background) enriched in $Z+\gamma$ and $W+\gamma$ processes. Monte Carlo (MC) simulations for these processes (SHERPA [12]) are normalized to data in these CRs and extrapolated to SR. In particular, two MC normalization factors (k_Z and k_W) for the two processes are introduced and they are determined from a simultaneous fit in all the regions (CRs and SR). The other background contributions, when possible, are estimated via data-driven methods. In particular the jet faking photon and the electron faking photon probability are known to be poorly described by MC therefore more precise data driven techniques have been developed. In the following sections both SR and CRs definitions are provided and the background estimation methods are explained.

5. – Signal region event selection

The analysis is performed on the full 8 TeV dataset ($20.3\,\mathrm{fb}^{-1}$). To select a sample of candidate events, a sequence of kinematic cuts is applied both on data and MC. Events were selected using an $E_{\mathrm{T}}^{\mathrm{miss}}$ trigger which requires $E_{\mathrm{T}}^{\mathrm{miss}} > 80\,\mathrm{GeV}$. Preselection cuts are required both in the SR and in CRs in order to select a sample of good quality events at the detector level. Only data collected in periods when all the subdetectors were working properly are considered and events where noise bursts in the EM calorimeter and data corruption occurred are rejected. Jets are required not to overlap with neither leptons nor photons. Events are required to have a reconstructed primary vertex with at least 5 associated tracks to reject non-collision background events. To the resulting ensemble of events the analysis cuts are applied to select SR events.

The SR is defined by requiring $E_{\mathrm{T}}^{\mathrm{miss}} > 150\,\mathrm{GeV}$ and a photon with $p_T^{\gamma} > 125\,\mathrm{GeV}$ and $|\eta^{\gamma}| < 1.37$. The leading photon must be well separated from $E_{\mathrm{T}}^{\mathrm{miss}}$ in order to avoid events in which fake $E_{\mathrm{T}}^{\mathrm{miss}}$ is caused by the partial loss of a photon, hence $\Delta\Phi(\gamma, E_{\mathrm{T}}^{\mathrm{miss}}) > 0.4$ is required. Events where more than one jet with $p_{\mathrm{T}} > 30\,\mathrm{GeV}$ is reconstructed are vetoed, if the jet is present it must be well separated from $E_{\mathrm{T}}^{\mathrm{miss}}$ to avoid fake $E_{\mathrm{T}}^{\mathrm{miss}}$ events ($\Delta\Phi(jet, E_{\mathrm{T}}^{\mathrm{miss}}) > 0.4$). A lepton veto is applied: no electron (with $p_{\mathrm{T}} > 7\,\mathrm{GeV}$ and $\eta < 2.47$) and no muon (with $p_{\mathrm{T}} > 6\,\mathrm{GeV}$ and $\eta < 2.5$) must be reconstructed in the event.

6. – Control regions definitions

Control regions are background-enriched regions where the presence of the signal is minimized while the presence of a certain background is maximized. CRs are chosen in order to not overlap to the SR and to maximize the fraction of a certain background. For this purpose, usually they are constructed by inverting a SR cut. Three different CRs are considered in this analysis: $Z(\to \mu\mu)+\gamma$ enriched CR (2μCR), $Z(\to ee)+\gamma$ enriched CR (2eleCR) and $W+\gamma$ enriched CR (1μCR). All these three regions are defined by reversing the SR lepton veto and requiring exactly two muons, two electrons or one muon, respectively. These leptons are required to be reconstructed with the same criteria of the vetoed leptons in SR. In addition, the lepton must be associated with an ID isolated track and $\Delta R(lepton, \gamma) > 0.5$. The photon pseudorapidity is relaxed with respect to the signal region selection ($|\eta^{\gamma}| < 2.37$, excluding the crack region).

Another CR has been used to study the $\gamma + jet$ background, as discussed in sect. **6**˙3.

6˙1. *Electron faking photon.* – As electrons and photons have a similar signature in the EM calorimeter, and converted photons could leave one or two tracks in the ID, there is a certain probability that an electron is reconstructed as energetic photon and therefore generates a fake event in the SR. Therefore the electron fake rate (defined precisely as the probability of reconstructing a photon from a true electron divided by the probability of reconstructing an electron from a true electron) is measured and it is multiplied by the number of events reconstructed in a mono-electron region (*i.e.* a region similar to the monophoton SR except that a single electron is required instead of a photon). The electron faking photon rate is measured through a data driven method (the so called *tag-and-probe* method) which consist in selecting a sample of events with one good electron of $E_T > 20\,\mathrm{GeV}$ (*tag*), an electron or a photon with $E_T > 125\,\mathrm{GeV}$ (*probe*) and $E_{\mathrm{T}}^{\mathrm{miss}} < 40\,\mathrm{GeV}$. The invariant mass of the tag and probe particles is required to be compatible with the Z mass. The electron fake rate is defined as the ratio between the number of probe photons and that of probe electrons.

6˙2. *Jet faking photon.* – The jet faking photon background comes from events where a high energetic jet is reconstructed as a tight and isolated photon. The so-called *two dimensional Sideband Method* (2DSideband) [13] is used to estimate this contribution. It is a data-driven technique which allows to estimate the amount of background contamination in a given region extracting it from three control regions. Photon candidates are placed in a plane (X, Y) where the X-axis is defined by the photon isolation energy and the Y-axis is defined by the photon identification tightness. The Y-axis is split into two bins: a bin with photon candidates that pass all the tight selection criteria, and a bin with photons which fail one or more cuts (referred to as *non-tight photons*). On the X-axis two regions are used in the measurement: a non-isolated bin

($10\,\text{GeV} < E_T^{iso} < 45\,\text{GeV}$) and an isolated bin ($E_T^{iso} < 5\,\text{GeV}$). The intermediate region ($5 < E_T^{iso} < 10\,\text{GeV}$) is ignored and is considered as a safety gap between the isolated and non isolated region in order to reduce the signal leakage (*i.e.* a fraction of tight and isolated photons which can leak into the three control regions) in the non isolated control regions. The region where $E_T^{iso} > 45\,\text{GeV}$ is assumed to contain only background. If N_A, N_B, N_C, N_D are the number of events entering, respectively, region A (region of the plane of tight and isolated photons), B (non-tight photons and isolated), C (photons non-tight and non-isolated), D (photons tight and non-isolated), then N_A^{bkg} is defined as the background contamination (*i.e.* fake photons) and N_A^{sign} the real signal (*i.e.* tight and isolated real photons). Assuming that the background isolation distribution does not depend on photon identification criteria, (this implies that the correlation between isolation and identification variables is negligible) and that the leakage of real photons in control regions B, C, D is negligible, the background contamination is given by

$$N_A^{bkg} = N_B^{bkg}\frac{N_D^{bkg}}{N_C^{bkg}} = N_B\frac{N_D}{N_C}. \tag{1}$$

To take into account the signal leakage contribution, the signal yield in each control region is subtracted from N_B, N_C and N_D. MC samples are used to compute the fraction of signal leakage in regions B, C, D which can be expressed in form of the following signal leakage coeffcients: $c_B = \frac{N_B^{sign,MC}}{N_A^{sign,MC}}$, $c_C = \frac{N_C^{sign,MC}}{N_A^{sign,MC}}$, $c_D = \frac{N_D^{sign,MC}}{N_A^{sign,MC}}$. With simple computations it is possible to show that the number of signal events corrected by the signal leakage is given by the following equation:

$$N_A^{sign} = N_A - N_B^{bkg}\frac{N_D^{bkg}}{N_C^{bkg}} = N_A - \left(N_B - N_A^{sign}c_B\right)\frac{N_D - N_A^{sign}c_D}{N_C - N_A^{sign}c_C}. \tag{2}$$

Results from the 2DSideband method should be independent on the choiche of regions B, C and D. Hence, a systematic uncertainty depending on the choice of their definition is estimated by relaxing the photon identification selection criteria and by varying the definition of the non-isolated region.

The method has been validated and it has been verified that signal MC isolation distribution well describes data signal isolation distribution. The background contamination in the 1μCR, 2μCR, 2eleCR and SR is shown in table I.

6˙3. *γ + jet background.* – The γ + jet events enter the SR if the jet is badly reconstructed and partially lost making high fake $E_{\text{T}}^{\text{miss}}$, while di-jets processes mimic SR events if one jet is misreconstructed as a photon and the other jet is badly reconstructed resulting in high fake $E_{\text{T}}^{\text{miss}}$. This background is expected to be very low because in the SR the jet is required to be well separated from the $E_{\text{T}}^{\text{miss}}$ ($\Delta\Phi(\text{jet}, E_{\text{T}}^{\text{miss}}) > 0.4$) precisely to avoid events in which $E_{\text{T}}^{\text{miss}}$ is caused by the partial loss of a jet.

This contamination is estimated with MC samples and a data-driven approach is used as a cross-check.

MC estimation. The MC estimation is computed using PYTHIA γ + jet samples and gives $\sim 0.38 \pm 0.21(\text{stat})^{+0.12}_{-0.34}(\text{syst})$ events in the SR. The systematic error is computed by varying each source of systematic uncertainties related to the energy/momentum

TABLE I. – *Estimation of N_A^{sign} and N_A^{bkg} corrected by signal leakage contribution.*

Region	γ selection	N_A^{sign}	N_A^{bkg}
SR	$p_T^\gamma > 125\,\text{GeV}$ $\lvert\eta^\gamma\rvert < 1.37$	505.35 $\pm 24.09 \pm 4.56$	15.65 $\pm 3.76 \pm 4.56$
$1\,\mu$CR	$p_T^\gamma > 125\,\text{GeV}$ $\lvert\eta^\gamma\rvert < 2.37$	325.85 $\pm 19.25 \pm 3.04$	14.15 $\pm 3.47 \pm 3.04$
$2\,\mu$CR	$p_T^\gamma > 125\,\text{GeV}$ $\lvert\eta^\gamma\rvert < 2.37$	69.96 $\pm 8.89 \pm 3.50$	1.04 $\pm 0.61 \pm 3.50$
$2\,ele$CR	$p_T^\gamma > 125\,\text{GeV}$ $\lvert\eta^\gamma\rvert < 2.37$	59.19 $\pm 8.20 \pm 0.77$	1.81 $\pm 0.51 \pm 0.77$

scale of the reconstructed objects and their identification, reconstruction and selection efficiencies, overall uncertainties (trigger, luminosity) on selection efficiency.

Data-driven estimation. The data-driven method adopted to cross-check the MC estimation is described below. Events with a jet of $p_T > 30\,\text{GeV}$ which is not well-separated from E_T^miss are vetoed (sect. **5**); only $\gamma +$ jet events with a badly recontructed jet with $p_T < 30\,\text{GeV}$ could enter the SR. A control region is defined by requiring all the cuts as in the SR (sect. **5**) but reversing the $\Delta\Phi(\text{jet}, E_\text{T}^\text{miss})$ cut. In this way, asking for $\Delta\Phi(\text{jet}, E_\text{T}^\text{miss}) < 0.4$, pathological events in which the jet is aligned to the E_T^miss are selected. From these events the electroweak background, coming from $W/Z +$ jet and $W/Z + \gamma$ processes, needs to be subtracted. MC simulation is used to subtract electroweak backgrounds. The MC samples used to simulate the electroweak background are SHERPA samples. The $\gamma +$ jet and di-jet contribution in the SR is estimated from the resulting jet p_T distribution by extrapolating it to the low ($< 30\,\text{GeV}$) jet p_T region. The estimation from data is compatible with the MC prediction.

7. – Simultaneous fit

$Z(\to \nu\nu) + \gamma$, $Z(\to ll) + \gamma$ and $W(\to l\nu) + \gamma$ processes are estimated performing a simultaneous fit in all CRs. A likelihood function is built assuming that the number of events in each region is described by a Poissonian function (P):

$$\prod_i P(N_{R_i}^{obs} | \mu \times N_{R_i}^{exp,\ sign} + k_Z \times N_{R_i}^{exp,\ Z+\gamma} + k_W \times N_{R_i}^{exp,\ W+\gamma} + N_{R_i}^{others}); \tag{3}$$

where i runs on the regions (CRs and SR), $N_{R_i}^{obs}$ is the number of observed events in data in each region, μ is a free parameter called signal strength, $N_{R_i}^{exp,\ sign}$ is the number of expects signal events from MC, $N_{R_i}^{others}$ is the number of expected events which do not have to be normalized in CRs (data driven estimation or purely MC estimation

TABLE II. – *The predicted total background from the simultaneous fit in CRs and the observed events in data are shown both for VR and for SR. The uncertainties associated to each event yield are statistical and systematic. For the $\gamma + jet$ the total uncertainty is shown.*

Process	Event yield (SR)	Event yield (VR)
$Z(\to \nu\nu) + \gamma$	$389 \pm 36 \pm 10$	$153 \pm 16 \pm 10$
$W(\to l\nu) + \gamma$	$82.5 \pm 5.3 \pm 3.4$	$67 \pm 5 \pm 5$
$W/Z + jet, t\bar{t}$, diboson	$83 \pm 2 \pm 28$	$47 \pm 2 \pm 14$
$Z(\to ll) + \gamma$	$2.0 \pm 0.2 \pm 0.6$	$2.9 \pm 0.3 \pm 0.6$
$\gamma +$ jet	$0.4^{+0.3}_{-0.4}$	$2.5^{+4.0}_{-2.5}$
Total background	$557 \pm 36 \pm 27$	$272 \pm 17 \pm 14$
Data	521	307

such as $\gamma + jet$ background); $N^{exp}_{R_i}$ is the expected (MC) yield for each of the $Z/W + \gamma$ background, rescaled by a factor k_Z or k_W. The systematic uncertainties are introduced in the model via nuisance parameters and their correlations are taken into account.

7˙1. *Validation region.* – The fit has been validated in a Validation Region (VR) which has been chosen as much as possible similar to the SR in background composition and statistical power but with a small signal contamination. Events are selected as in the SR except for the request of a lower $E_{\mathrm{T}}^{\mathrm{miss}}$ ($110 < E_{\mathrm{T}}^{\mathrm{miss}} < 150\,\mathrm{GeV}$) and a larger photon pseudorapidity ($|\eta^{\gamma}| < 2.37$) to enhance the number of events. A cut on the azimuthal separation between the photon and the jet is applied to make the VR similar in background concentration to the SR ($\Delta\Phi(\gamma, jet) < 2.7$). To minimize the signal yield a request on the azimuthal separation between the photon and the $E_{\mathrm{T}}^{\mathrm{miss}}$ has been applied ($\Delta\Phi(\gamma, E_{\mathrm{T}}^{\mathrm{miss}}) < 3.00$).

7˙1.1. Low $E_{\mathrm{T}}^{\mathrm{miss}}$ Control Regions. The simultaneous fit is performed in the VR using three low $E_{\mathrm{T}}^{\mathrm{miss}}$ CRs. These CRs are similar to the $W\gamma$, $Z(\to \mu\mu) + \gamma$ and $Z(\to ee) + \gamma$ enriched CRs defined in sect. **6** apart from the $E_{\mathrm{T}}^{\mathrm{miss}}$ cut. These low $E_{\mathrm{T}}^{\mathrm{miss}}$ CRs are defined by $110 < E_{\mathrm{T}}^{\mathrm{miss}} < 150\,\mathrm{GeV}$. Neither the $\Delta\Phi(\gamma, jet) < 2.7$ nor the $\Delta\Phi(\gamma, E_{\mathrm{T}}^{\mathrm{miss}}) < 3.00$ has been applied in these CRs. The $\Delta\Phi(\gamma, E_{\mathrm{T}}^{\mathrm{miss}})$ has not been applied because it reduces too much the number of selected events. No biases are expected because the $\Delta\Phi(\gamma, E_{\mathrm{T}}^{\mathrm{miss}})$ distributions have been checked to be similar in data and MC simulations.

7˙1.2. Fit validation. All the background contributions, apart from $Z/W + \gamma$, are estimated as in the SR and are used as inputs to the fit. The fit has been performed in the VR using the low-$E_{\mathrm{T}}^{\mathrm{miss}}$ CR. 307 events are observed in data and $272 \pm 17 \pm 14$ are predicted by the fit (table II). Results from fit show agreement between the fitted background and the data observation within 2σ.

8. – Results

521 events are observed in data SR. A simultaneous fit using CRs predicts $557 \pm 36(\mathrm{stat}) \pm 27(\mathrm{syst})$ SM events in SR (table II), the total systematic uncertainty on the

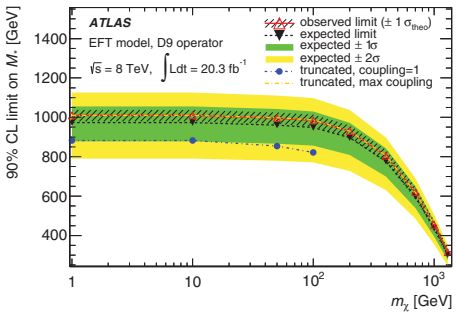

Fig. 2. – 90% CL limits on the EFT WIMP model parameter M^* for a number of Dark Matter masses m_χ ranging from 1 to 1300 GeV for the spin-dependent operator D9 [16].

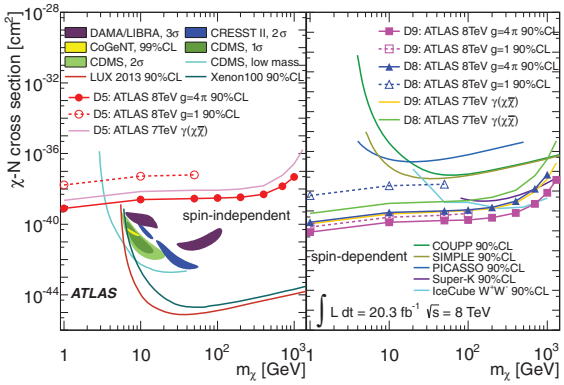

Fig. 3. – 90% CL limits on the $\chi-$nucleon cross-section as a function of m_χ [16].

background prediction is $\sim 5\%$ while the statistical $\sim 6\%$. In particular, among the main systematic uncertainties there is the uncertainty on the electron fake estimation, the uncertainty related to the reconstruction and identification of electrons and muons, and the electron/photon energy scale systematic uncertainty. Data agree with the SM expectation and no significant deviation is observed.

8˙1. *Model-independent limit.* – Results are interpreted by setting a model independent limit on the presence of new physics. The number of selected events coming from a potential new physics process of cross-section σ is $N_{new} = L \times \sigma \times A \times \epsilon$, where L is the integrated luminosity, $A \times \epsilon$ is the product of the acceptance of the selection (A) and the experimental efficiency to select signal events (ϵ). A conservative measure for the efficiency is estimated to be 69%. Without any hypothesis on the model of new physics, a limit on the fiducial cross-section $\sigma_{fid} = \sigma \times A$ is computed with a profiled likelihood ratio statistical test and CL_S technique [14] performed using both SR and CRs. The expected (observed) upper limit on σ_{fid} is 6.1 (5.3) fb at 95% CL.

8˙2. *Limits on WIMP direct production.* – Exclusion limits on WIMPs direct production in the framework of effective field theories are computed. In the framework of EFT, the interaction between incoming partons and WIMPs is parameterized by a reduced number of operators as an approximation for a full theory that includes Dark

Matter. The role of effective operators is to mimic the different nature of the mediators in a Fermi-like point interaction. I considered the D9 operator $(\bar{\chi}\sigma^{\mu\nu}\chi\bar{f}\sigma_{\mu\nu}f)$, which represents a spin dependent tensor interaction between incoming fermions (f) and Dirac fermion WIMPs (χ). The cross-section of the interaction between the two incoming SM fermions and the two outgoing DM particles can be related to the parameter M^* via the relation $\sigma(ff \to \chi\chi) \propto \frac{g_{SM}^2 g_{DM}^2}{(Q_{tr}^2 - M_{mediator}^2)^2 + \Gamma^2 M_{mediator}^2} \Rightarrow \frac{g_{SM}^2 g_{DM}^2}{M_{mediator}^4} \Rightarrow \frac{1}{M^{*4}}$, if the momentum exchanged in the interaction is $Q_{tr} < \sqrt{g_{SM} g_\chi} M^*$. Hence, an upper exclusion limit on the suppression scale M^* as a function of the WIMP mass (m_χ) can be set. The EFT set of WIMP + γMC samples have been generated for WIMP masses of 10 GeV, 50 GeV, 100 GeV, 200 GeV, 400 GeV, 700 GeV, 1000 GeV and 1300 GeV and for $M^* = 1$ TeV. The limit on M^* is computed considering systematics on the Standard Model background and on the WIMP signal. Events which do not fulfill the EFT validity requirement ($Q_{tr} < \sqrt{g_{SM} g_\chi} M^*$) if the coupling is unity (g_{SM}, g_χ =1) or if the coupling is 4π (g_{SM}, $g_\chi = 4\pi$) have been rejected. Upper limits at 90% CL are set on M^* for each m_χ for the D9 operator (fig. 2). To directly compare results with Direct Detection experiments, the M^* limits can be converted into χ–nucleon scattering cross-sections using the following relation [15]: $\sigma^{D9} = 4.7 \times 10^{-39}\,\mathrm{cm}^2 \left(\frac{\mu_\chi}{1\,\mathrm{GeV}}\right)^2 \left(\frac{300\,\mathrm{GeV}}{M^*}\right)^4$ where μ_χ is the reduced mass of χ-nucleon system. The limits at 90% CL on the χ-nucleon scattering cross-sections are reported in fig. 3 for the D9 operator.

9. – Conclusion

A search for dark matter production at the LHC has been performed on the full 8 TeV dataset collected by the ATLAS detector. The monophoton plus missing transverse momentum final state has been investigated. The SM processes with a monophoton final state has been estimated and has been compared to the observed data. No significant excess between observation in data and the predicted SM processes has been found. Results are interpreted by setting a model independent limit on the presence of new physics and limits in the context of EFT WIMP production.

REFERENCES

[1] Bertone G., Hooper D. and Silk J., *Phys. Rep.*, **405** (2005) 279.
[2] The ATLAS Collaboration, *The ATLAS Experiment at the CERN Large Hadron Collider JINST*, **3** (2008) S08003.
[3] The CMS Collaboration, *The CMS experiment at the CERN LHC JINST*, **3** (2008) S08004.
[4] The LHCb Collaboration, *The LHCb detector at the LHC JINST*, **3** (2008) S08005.
[5] The ALICE Collaboration, *The ALICE experiment at the CERN LHC JINST*, **3** (2008) S08002.
[6] The ATLAS Collaboration, *The ATLAS Inner Detector commissioning and calibration Eur. Phys. J. C*, **70** (2010) 787.
[7] The ATLAS Collaboration, *Electron and photon energy calibration with the ATLAS detector using LHC Run 1 data Eur. Phys. J. C*, **74** (2014) 3071; CERN-PH-EP-2014-153.
[8] The ATLAS Collaboration, *Electron and photon reconstruction and identification in ATLAS: expected performance at high energy and results at 900 GeV*, ATLAS-CONF-2010-0052010.
[9] Cacciari M., Salam G. P. and Soyez G., *JHEP*, **04** (2008) 801; arXiv:0802.1189.
[10] The ATLAS Collaboration, *Eur. Phys. J. C*, **74** (2014) 3130; arXiv:1407.3935 (2014).

[11] The ATLAS Collaboration, *ATLAS-CONF-2013-082*, `http://cdsweb.cern.ch/record/1570993` (2013).
[12] Gleisberg T. *et al.*, *JHEP*, **02** (2009) 007.
[13] The ATLAS Collaboration, *Evidence for prompt photon production in pp collisions at* $\sqrt{s} = 7$ *TeV with the ATLAS detector* ATLAS-CONF-2010-077 (2010).
[14] Read L., *Presentation of search results: The CL(s) technique*, *J. Phys. G*, **28** (2002) 2693.
[15] Bai Y., Fox P. and Harnik R., *The Tevatron at the frontier of dark matter direct detection JHEP*, **12** (2010) 048; arXiv:1005.3797.
[16] The ATLAS Collaboration, *Search for new phenomena in events with a photon and missing transverse momentum in pp collisions at* $\sqrt{s} = 8$ *TeV with the ATLAS detector Phys. Rev. D*, **91** (2015) 012008.